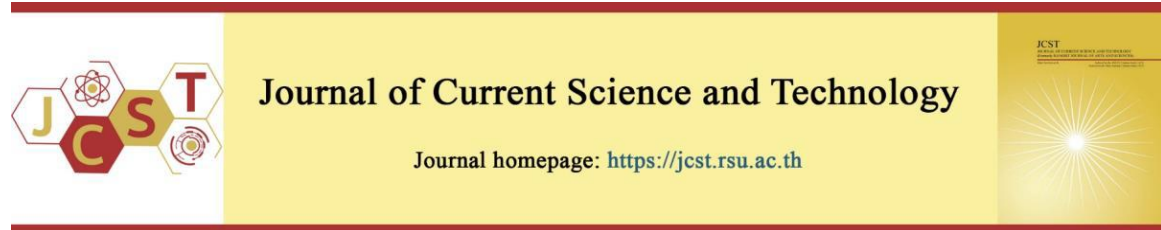


Cite this article: Nguyen, X. V., & Nguyen, N. L. (2024). Automated inverse kinematics configuration selection for path planning of a 6-DOF robot. *Journal of Current Science and Technology*, 14(1), Article 10. <https://doi.org/10.59796/jcst.V14N1.2024.10>



Automated Inverse Kinematics Configuration Selection for Path Planning of a 6-DOF Robot

Xuan-Vinh Nguyen^{1,2*} and Ngoc-Lam Nguyen³

¹Faculty of Electronics and Telecommunications, University of Science, Ho Chi Minh City, Vietnam

²Vietnam National University, Ho Chi Minh City, Vietnam

³Vietnam Research Institute of Electronics, Informatics and Automation

*Corresponding author; E-mail: nxvinh@hcmus.edu.vn

Received 12 June, 2023; Revised 4 September, 2023; Accepted 29 September, 2023

Published online 6 December, 2023

Abstract

This article presents an automated technique for selecting suitable inverse configurations for the path planning of robots with six degrees of freedom (6 DOF). Traditionally, robots were limited to a single fixed configuration for movement, but now there's a growing need for robots that can adapt to different situations, especially in unknown environments. In this study, we introduce an innovative approach designed to assist a small industrial robot known as AKB-IRV1. This approach helps the robot determine and automatically select the most suitable configuration to move, which is essential for effective path planning. We simplify a complex problem related to how the robot's joints work through geometric analysis, breaking it down into two stages: calculation and selection of the best joint angles for movement. We also use computer simulations to assess the robot's workspace, considering joint angles as constraints. Our findings reveal that taking joint angles into account significantly reduces the robot's effective workspace. We also present a method for the robot to automatically choose the right configuration when planning its path, especially in uncertain situations. This ability allows the robot to change its configuration as needed, aligning with the goal of minimizing configuration changes. This method has promising applications for intelligent robots operating in unfamiliar environments.

Keywords: 6-DOF robot; kinematics; workspace; path planning

Nomenclature

Symbol	Description
ψ, θ, ϕ	Roll, Pitch, Yaw angle
n, s, a	Orthogonal vectors represent the orientation
p	Position vector
θ_i	Joint angle boundary
α_i	Connecting rod torque
a_i	Connecting rod length
d_i	Joint offset
A_{i-1}^i	Homogeneous transformation matrix
$R_{(\phi, \theta, \psi)}$	Rotation matrix

1. Introduction

Industrial robots have gradually replaced humans in manufacturing processes, particularly in modern and mass production lines requiring high accuracy and repetition, such as car production, welding, cutting, and metal processing. An industrial robot requires a minimum number of degrees of freedom to accommodate movement in the three positional and three manipulator directions. Because of their adaptability, six-degree-of-freedom (6-DOF) robots are widely used in industry. In production systems, these robots primarily perform programmed operations along known and repetitive trajectories. When training and configuring the robot, experts will analyze the

motion process and choose a suitable inverse kinematic configuration based on personal experience. When performing repetitive operations in a fixed workspace, the 6-DOF robot will default to the chosen configuration (Craig, 2005; Spong et al., 2020).

Kinematic problems are used to represent the parameters at the joints associated with the robot configurations. When the positions of the joints are known, the forward kinematics problem is used to determine the position and orientation of the manipulator (Spong et al., 2004). The Denavit-Hartenberg method is a popular method for solving the forward kinematics problem for robots. Meanwhile, when the position and angle of the manipulator are known, the inverse kinematics problem is used to find matching variables (Denavit, & Hartenberg, 1955; Hartenberg, & Denavit, 1964).

Finding the joint variables for the 6-DOF robot to move the impact head to the desired position for the inverse kinematics problem is quite challenging. The 6-DOF robot will be able to have more than one inverse kinematic configuration (the solution set) at a different end-effector position and orientation. The multi-solution problem's interdependent results continue to be a significant obstacle. The existence of multiple solutions and singularities makes it quite difficult to solve inverse kinematics for a 6-DOF robot (Hayes et al., 2003; Husi, 2015).

As a general rule, the geometric method is frequently used in inverse kinematics (Spong et al., 2020). However, finding a suitable configuration for the 6-DOF robot remains severely constrained by the interdependent outcomes of the multi-solution problem. Lee, & Ziegler (1984) proposed a geometric solution for the 6-axis Puma 560 robot joints using additional directions of the robot arm position. This solution has four joint solutions for the first three joints and two possible solutions for the last three joints. According to Wang et al. (2017), there are three robot configuration indicators (arm, elbow, and wrist), and the one-dimensional search problem for the fifth joint angle is the focus of inverse kinematics. Chen et al. (2015) used screw theory to address the 6-DOF robot's inverse kinematics problem.

Aside from classic inverse kinematics solutions, newly published studies have presented numerous different approaches based on machine learning (Wang et al., 2020; Tagliani et al., 2022),

the Particle Swarm Optimization (PSO) algorithm (Yiyang et al., 2021), Behavior Tree (Zhang, & Hannaford, 2019), and Artificial Neural Networks (ANN) algorithms (Kshitish et al., 2017; Ahmed et al., 2016; Abderrahim et al., 2023).

For redundant manipulator path planning, inverse kinematics are the main issue. The set of points and orientations of the end-effector is defined for the robot's trajectory control. The joint angles will be computed at each location and orientation of the end-effector, allowing numerous robot configurations to be established. On the contrary, each manipulator configuration will have a different operating region in space (Iqbal et al., 2012; Isiah, & Luis, 2017). While following a smooth intended end-effector trajectory, a primary configuration with the maximum workspace is usually considered. Sometimes the trajectory path extends beyond the workspace or does not fully match the primary configuration. In this situation, switching the relevant configurations is required to assure the tracking of the robot's trajectory. Minimizing the number of configuration transitions is necessary to minimize robot operation time and energy. Additionally, since the inverse kinematics problem for a 6-DOF manipulator has multiple solutions, selecting the right configurations is essential for trajectory planning (Perumaal, & Jawahar, 2012; Siméon et al., 2004).

Path planning is a critical issue in the field of robot control. Path planning algorithms generate a geometric path for the manipulator end-effector from the starting point to the ending point, passing through pre-defined via-points in the robot's workspace. Trajectory planning algorithms follow a specific geometric path and control the movement of the end-effector with time information. When working in a hostile environment, the robot must plan this path automatically and efficiently based on minimum execution time, energy, and jerk (Perumaal, & Jawahar, 2012; Gasparetto et al., 2015).

In robot path planning, it's vital to define the workspace for each inverse configuration. This is especially important when dealing with various inverse kinematic setups that can lead to discontinuous path segments. To tackle scenarios with obstacles, it's crucial to determine via-points within the manipulator's workspace before constructing the path. This approach aligns with the perspectives of Perumaal, & Jawahar (2012) and Siméon et al. (2004).

With the development of applications such as intelligent robots, robots will be able to adjust the operating program to respond appropriately to working environment parameters. In uncertain environments, robots must be able to change operating configurations automatically while in operation. As a result, the fixed selection of current inverse kinematic configurations is no longer sufficient. According to Chembuly, & Voruganti (2020), these robots must be able to recognize and autonomously select the best operating configuration for reality.

Previous studies have delved into inverse kinematics, robot path planning, and 6-degree-of-freedom robot working areas. Yet, there's a gap in research that tackles the holistic challenge of solving inverse kinematics, considering mechanical constraints for workspace definition, path planning, and automating the selection of appropriate inverse configurations for these robots.

This study introduces an autonomous approach for 6-DOF robots to select the best configuration during various path processes. Section 2 presents the results of our inverse kinematics analysis, where we use the Denavit-Hartenberg (D-H) method for forward kinematics and a two-stage geometric approach (end-effector position and orientation) for inverse kinematics. In Section 3, we examine the 6-DOF robot's workspace, considering both position and orientation criteria while accounting for joint mechanical limits. In Section 4, we test the configurations for inverse kinematics by proposing a smooth end-effector path that includes sections beyond the primary configuration's range. We use a

criterion-based configuration selection method to minimize switching while maintaining position and orientation. Our results demonstrate the feasibility of switching between suitable configurations and accommodating trajectory paths beyond a configuration's workspace. Section 5 concludes the paper.

2. Kinematic model

Kinematics involves two components: forward and inverse. Forward kinematics aims to find the end-effector's position and orientation using joint angles and lengths. In contrast, inverse kinematics finds joint angles when the end-effector's position and orientation, along with joint lengths, are known.

2.1 Geometric model

The 6-DOF manipulator platform used in this paper is a small serial chain robot named AKB-IRV1, developed by AKB Machinery Company, Vietnam (AKB Machinery, n.d.). This robot has an articulated structure, a maximum payload of 48 kg, a maximum reach of 725 mm, an accuracy repeatability of ± 0.02 mm, a power consumption of 0.5 KVA, and an approximate weight of 75 kg. As shown in Figure 1, the robot AKB-IRV1 is made up of six revolute joints and a gripper. Each module has a built-in DC servo motor with a position and velocity controller. The AKB-IRV1's structure is similar to that of the KUKA KR-15/2 robot (Gracia et al., 2009) and has the coordinate frame locations shown in Figure 2. The robot has Denavit-Hartenberg parameters due to the manipulator configuration shown in Table 1.



Figure 1 The AKB-IRV1 robot

Table 1 AKB-IRV1 robot link coordinate parameters with joint angles limit

Joint i	α_i	a_i (mm)	d_i (mm)	θ_i	θ_{imin} (degree)	θ_{imax} (degree)
1	$\pi/2$	100	370	θ_1	-132	+ 132
2	0	300	0	θ_2	-90	+ 90
3	$\pi/2$	111.36	0	θ_3	-90	+ 60
4	$-\pi/2$	0	300	θ_4	-130	+ 130
5	$\pi/2$	0	0	θ_5	-100	+ 100
6	0	0	105	θ_6	-180	+ 180

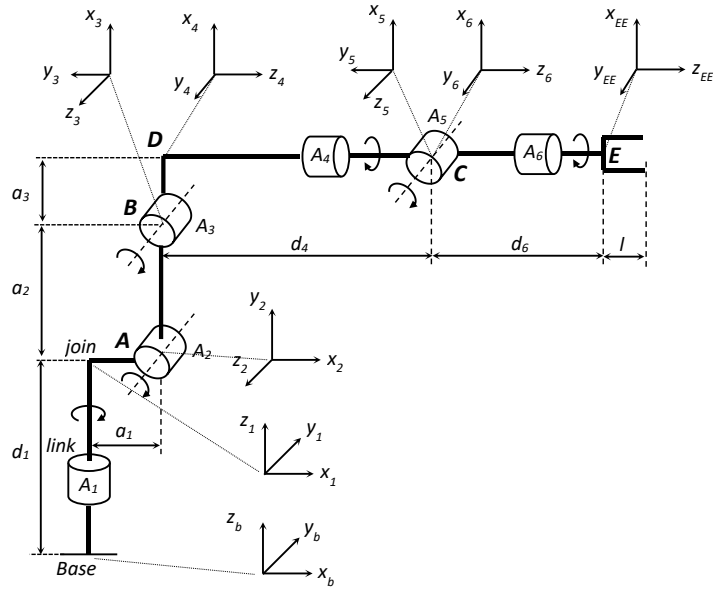


Figure 2 Link coordinate parameter system of the AKB-IRV1 ($\theta_2 = \pi/2$)

Following Spong et al. (2004), the six homogeneous transformation matrices A_{i-1}^i for the AKB-IRV1 robot shown in Figure 2 are given in Equation (1):

$$A_{i-1}^i = \begin{bmatrix} c\theta_i & -s\theta_i c\alpha_i & s\theta_i s\alpha_i & a_i c\theta_i \\ s\theta_i & c\theta_i c\alpha_i & -c\theta_i s\alpha_i & a_i s\theta_i \\ 0 & s\alpha_i & c\alpha_i & d_i \\ 0 & 0 & 0 & 1 \end{bmatrix} \quad (1)$$

where

$$c\alpha_i \equiv \cos(\alpha_i); s\alpha_i \equiv \sin(\alpha_i);$$

$$c\theta_i \equiv \cos(\theta_i); s\theta_i \equiv \sin(\theta_i); (i=1,2,\dots,6)$$

α_i : The angle from \hat{Z}_i to \hat{Z}_{i+1} measured along \hat{X}_i

a_i : The distance from \hat{Z}_i to \hat{Z}_{i+1} measured along \hat{X}_i

d_i : The distance from \hat{X}_{i-1} to \hat{X}_i measured along \hat{Z}_i

θ_i : The angle from \hat{X}_{i-1} to \hat{X}_i measured along \hat{Z}_i

2.2 Forward kinematic

In Lee, & Ziegler's (1984) forward kinematics work, Equation (2) introduced the transformation matrix. This matrix determines the end-effector's position and orientation relative to the robot's base coordinate system, encapsulating their spatial relationship.

$$T_0^6 = A_0^1 A_1^2 A_2^3 A_3^4 A_4^5 A_5^6$$

$$T_0^6 = \begin{bmatrix} n_x & s_x & a_x & p_x \\ n_y & s_y & a_y & p_y \\ n_z & s_z & a_z & p_z \\ 0 & 0 & 0 & 1 \end{bmatrix} = \begin{bmatrix} R_0^6 & P_0^6 \\ 0 & I \end{bmatrix} \quad (2)$$

The end-effector's orientation is defined by the vectors n , s , and a , and its position is represented by p . Together, these vectors describe the end-effector's spatial configuration relative to the base coordinate system. In Figure 2, the end-effector (point E) matrix is given as follows:

$$E_6 = \begin{bmatrix} u_x & v_x & w_x & q_x \\ u_y & v_y & w_y & q_y \\ u_z & v_z & w_z & q_z \\ 0 & 0 & 0 & 1 \end{bmatrix} \quad (3)$$

The wrist position p_x, p_y, p_z can be found using;

$$\begin{bmatrix} p_x \\ p_y \\ p_z \\ 1 \end{bmatrix} = \begin{bmatrix} q_x - d_6 w_x \\ q_y - d_6 w_y \\ q_z - d_6 w_z \\ 1 \end{bmatrix} \quad (4)$$

The wrist orientation and position (point C in Figure 2) are defined by Equation (5).

$$W_6 = \begin{bmatrix} u_x & v_x & w_x & p_x \\ u_y & v_y & w_y & p_y \\ u_z & v_z & w_z & p_z \\ 0 & 0 & 0 & 1 \end{bmatrix} \quad (5)$$

2.3 The inverse forward kinematics problem

The inverse kinematics problem for a 6-DOF manipulator involves finding the joint angles that correspond to a given end-effector position and orientation. This is a multi-solution challenge with various sets of solutions. Piotrowski and Barylski (2014) suggest breaking it down into two steps: first, solving the position inverse kinematics to determine the first three joint angles ($\theta_1, \theta_2, \theta_3$), and then addressing the orientation inverse kinematics to calculate the last three joint angles

($\theta_4, \theta_5, \theta_6$). This division simplifies the overall kinematic analysis. Inverse kinematics problems focus on the wrist coordinates of the manipulator and start by determining the wrist's position and angle based on the manipulator's given coordinates and position using Equation (5).

2.3.1 Inverse position kinematic

In Figure 3, when considering the manipulator perpendicularly onto the Oxy plane, the wrist position (point C) creates two pairs of points A and B. This results in two angles, θ_{11} and θ_{12} , for θ_1 . These angles represent the front and rear configurations, respectively, as calculated by Equation (6).

$$\theta_{11} = \tan^{-1} \left(\frac{p_y}{p_x} \right); \theta_{12} = \tan^{-1} \left(\frac{p_y}{p_x} \right) + \pi \quad (6)$$

When projecting the manipulator perpendicularly onto the $Oxyz$ plane, each θ_1 value from Equation (6) yields two pairs of angles, θ_2 and θ_3 . This results in four inverse kinematic configurations, as depicted in Figure 3. The geometric and trigonometric methods were employed to calculate θ_2 and θ_3 . Table 2 and Figure 4 illustrate the front-above, front-below, rear-above, and rear-below configurations corresponding to these angles (Lee, & Ziegler, 1984).

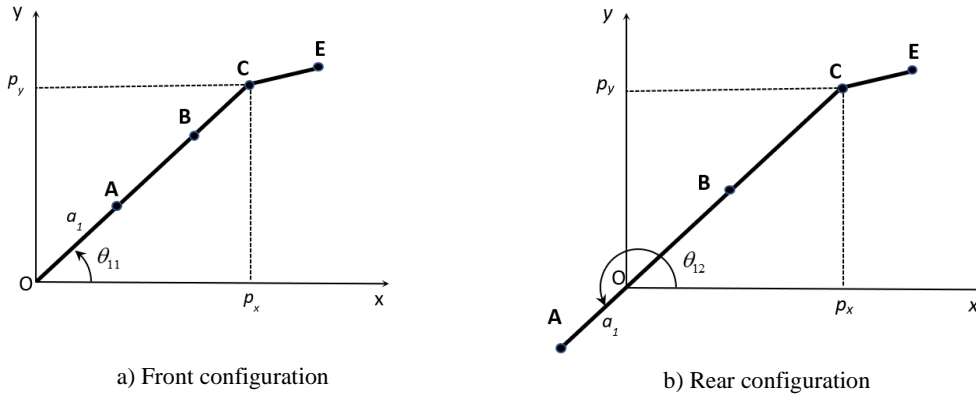


Figure 3 Joint angle θ_1 according to the position of point C on the Oxy plane

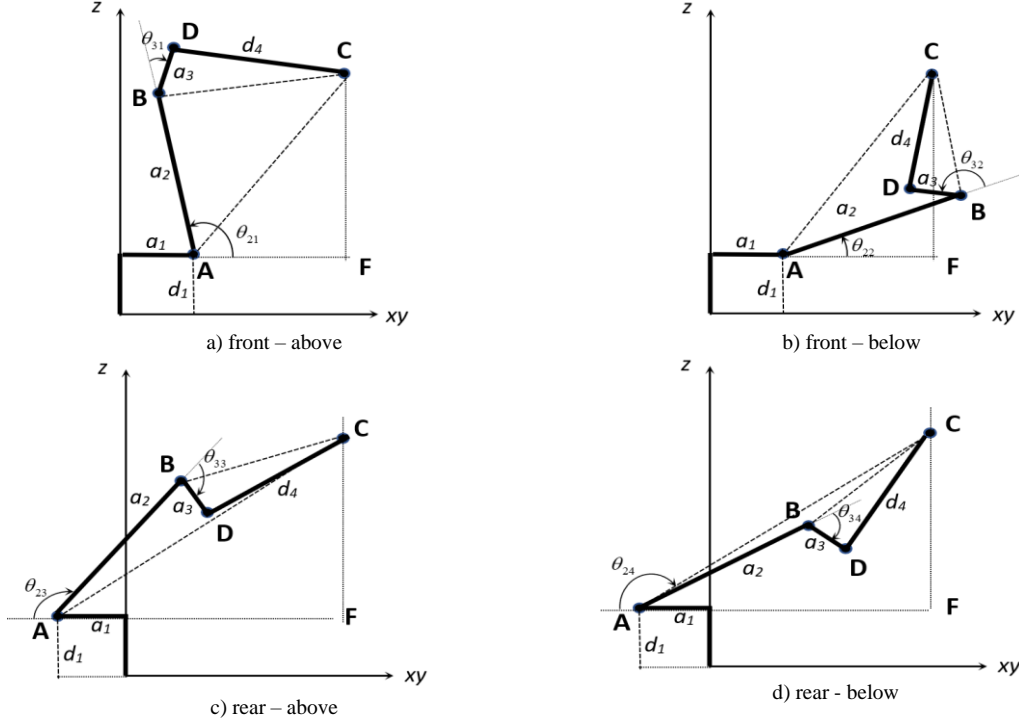


Figure 4 Four inverse configurations of the AKB-IVR1 robot

Table 2 The joint angle set for position inverse kinematics solutions

Configuration	θ_1	θ_2	θ_3
front - above	$\theta_{11} = \tan^{-1}\left(\frac{p_y}{p_x}\right)$	$\theta_{21} = \widehat{CAF} + \widehat{BAC}$	$\theta_{31} = \widehat{DBC} - (\pi - \widehat{ABC})$
front - below	$\theta_{11} = \tan^{-1}\left(\frac{p_y}{p_x}\right)$	$\theta_{22} = \widehat{CAF} - \widehat{BAC}$	$\theta_{32} = \widehat{DBC} + (\pi - \widehat{ABC})$
rear - above	$\theta_{12} = \tan^{-1}\left(\frac{p_y}{p_x}\right) + \pi$	$\theta_{23} = \pi - (\widehat{CAF} + \widehat{BAC})$	$\theta_{33} = \widehat{DBC} + (\pi - \widehat{ABC})$
rear - below	$\theta_{12} = \tan^{-1}\left(\frac{p_y}{p_x}\right) + \pi$	$\theta_{24} = \pi - (\widehat{CAF} - \widehat{BAC})$	$\theta_{34} = \widehat{DBC} - (\pi - \widehat{ABC})$

where:

$$\widehat{CAF} = \tan^{-1}\left(\frac{CF}{AF}\right); \widehat{BAC} = \cos^{-1}\left(\frac{a_2^2 + AC^2 - BC^2}{2a_2 \cdot AC}\right); \widehat{ABC} = \cos^{-1}\left(\frac{a_2^2 + BC^2 - AC^2}{2a_2 \cdot BC}\right); \widehat{DBC} = \tan^{-1}\left(\frac{d_4}{a_3}\right);$$

$$\text{and } BC = \sqrt{a_3^2 + d_4^2}; AC = \sqrt{AF^2 + CF^2}; \quad (7)$$

The inverse position kinematics problem has yielded four sets of matching angle solutions $(\theta_1, \theta_2, \theta_3)$. The next part of the inverse kinematics problem is to determine the matching angles $(\theta_4, \theta_5, \theta_6)$ based on the orientation angle of the robot.

2.3.2 Inverse orientation kinematics

Section 2.2.1 deals with the inverse position kinematics problem, solving for the first three joint

angles $(\theta_1, \theta_2, \theta_3)$ of the 6-DOF manipulator. For the remaining three joint angles $(\theta_4, \theta_5, \theta_6)$, we use the inverse kinematics problem with the provided wrist angle. This section outlines how to calculate these angles using the RPY rotation method, a common approach for describing manipulator angles (Spong et al., 2004). The resulting rotation matrix, RPY, is presented below:

$$R_{(\phi,\theta,\psi)} = R_z(\phi).R_y(\theta).R_x(\psi) = \begin{bmatrix} c\phi c\theta & c\phi s\theta s\psi - s\phi c\psi & c\phi s\theta c\psi + s\phi s\psi \\ s\phi c\theta & s\phi s\theta s\psi + c\phi c\psi & s\phi s\theta c\psi - c\phi s\psi \\ -s\theta & c\theta s\psi & c\theta c\psi \end{bmatrix} \quad (8)$$

where:

$$R_z(\phi) = \begin{bmatrix} c\phi & -s\phi & 0 \\ s\phi & c\phi & 0 \\ 0 & 0 & 1 \end{bmatrix}; R_y(\theta) = \begin{bmatrix} c\theta & 0 & s\theta \\ 0 & 1 & 0 \\ -s\theta & 0 & c\theta \end{bmatrix}; R_x(\psi) = \begin{bmatrix} 1 & 0 & 0 \\ 0 & c\psi & -s\psi \\ 0 & s\psi & c\psi \end{bmatrix} \quad (9)$$

The orientation inverse kinematics problem involves determining the RPY rotation angles (ψ, θ, ϕ) corresponding to the rotation matrix R_0^6 in Equation (2). The (ψ, θ, ϕ) values are matched by a directional angle matrix that represents spherical

rotations at the manipulator wrist frame. Since the first three angles $(\theta_1, \theta_2, \theta_3)$ have already been determined in Section 2.2.1, the rotation matrix R only needs to be represented with the unknown joint angles $(\theta_4, \theta_5, \theta_6)$.

From Equation (1):

$$R_0^1 = \begin{bmatrix} c\theta_1 & 0 & s\theta_1 \\ s\theta_1 & 0 & -c\theta_1 \\ 0 & 1 & 0 \end{bmatrix}; R_1^2 = \begin{bmatrix} c\theta_2 & -s\theta_2 & 0 \\ s\theta_2 & c\theta_2 & 0 \\ 0 & 0 & 1 \end{bmatrix}; R_2^3 = \begin{bmatrix} c\theta_3 & 0 & s\theta_3 \\ s\theta_3 & 0 & -c\theta_3 \\ 0 & 1 & 0 \end{bmatrix};$$

$$R_3^4 = \begin{bmatrix} c\theta_4 & 0 & -s\theta_4 \\ s\theta_4 & 0 & c\theta_4 \\ 0 & -1 & 0 \end{bmatrix}; R_4^5 = \begin{bmatrix} c\theta_5 & 0 & s\theta_5 \\ s\theta_5 & 0 & -c\theta_5 \\ 0 & 1 & 0 \end{bmatrix}; R_5^6 = \begin{bmatrix} c\theta_6 & -s\theta_6 & 0 \\ s\theta_6 & c\theta_6 & 0 \\ 0 & 0 & 1 \end{bmatrix} \quad (10)$$

The orientation matrix R_0^6 is given by Equation (11).

$$R_0^6 = R_0^1 R_1^2 R_2^3 R_3^4 R_4^5 R_5^6 = R_0^3 R_3^6 \quad (11)$$

Inverse orientation kinematics is about finding RPY angles that match a given rotation matrix R. The rotation matrix R_0^6 , obtained for wrist orientation, has the same format as the RPY transformation matrix $R_{(\phi,\theta,\psi)}$.

From Equations (9) and (10), the matrixes $R_{(\phi,\theta,\psi)}$ and R_0^6 can be compared as follows:

$$R_3^6 = (R_0^3)^{-1} R_0^6 = (R_0^3)^{-1} R_{(\phi,\theta,\psi)} \quad (12)$$

Equation (12) derives the matrix $(R_0^3)^{-1}$ from angles $\theta_1, \theta_2, \theta_3$, and matrix $R_{(\phi,\theta,\psi)}$ is defined by RPY angles. Therefore, it becomes possible to find the remaining corresponding angles $\theta_4, \theta_5, \theta_6$ from matrix R_3^6 as follows:

$$R_3^6 = \begin{bmatrix} c\theta_4 c\theta_5 c\theta_6 - s\theta_4 s\theta_6 & -c\theta_4 c\theta_5 s\theta_6 - s\theta_4 c\theta_6 & c\theta_4 s\theta_5 \\ s\theta_4 s\theta_5 c\theta_6 + c\theta_4 s\theta_6 & -s\theta_4 c\theta_5 s\theta_6 + c\theta_4 c\theta_6 & s\theta_4 s\theta_5 \\ -s\theta_5 c\theta_6 & s\theta_5 s\theta_6 & c\theta_5 \end{bmatrix} = (R_0^3)^{-1} R_{(\phi,\theta,\psi)} \quad (13)$$

From Equation (13), yield

$$\theta_5 = \tan^{-1} \left(\frac{\sqrt{1 - R_3^6(3,3)^2}}{R_3^6(3,3)} \right) \quad (14)$$

There are three solution sets for θ_4 and θ_6 that correspond to the values of $s\theta_5$

Case $s\theta_5 > 0$:

$$\theta_{41} = \tan^{-1} \left(\frac{R_3^6(2,3)}{-R_3^6(1,3)} \right);$$

$$\theta_{61} = \tan^{-1} \left(\frac{R_3^6(3,2)}{-R_3^6(3,1)} \right) \quad (15)$$

Case $s\theta_5 < 0$:

$$\theta_{41} = \tan^{-1} \left(\frac{R_3^6(2,3)}{R_3^6(1,3)} \right);$$

$$\theta_{61} = \tan^{-1} \left(\frac{-R_3^6(3,2)}{R_3^6(3,1)} \right) \quad (16)$$

$$\text{Case } s\theta_5 = 0: \theta_4 = 0; \theta_5 = 0; \theta_6 = 0 \quad (17)$$

In this section, we address the inverse kinematics problem of a 6-DOF robot, which has four solution sets, each corresponding to a different configuration with the same end-effector position and angle. The choice of coordinate systems at the joints plays a crucial role in the problem's complexity. By selecting suitable coordinate systems and breaking down the problem into two sequential stages, we've simplified the process of determining solution sets compared to traditional methods. The next section will define the

workspace and present simulation results for each configuration.

3. Simulation result

3.1 Inverse kinematics of a 6-DOF robot

In this section, we introduce the AKB-IRV1 manipulator model, defined by DH parameters in Table 1. We use a MATLAB simulation program to assess both forward and inverse kinematics, as described in Section 2.2, to examine the 6-DOF manipulator's characteristics and operability.

To visually confirm the kinematics problem, start by examining the manipulator with the end-effector in position C (0.12 m; -0.24 m; 0.82 m) and with orientations $(\psi_C, \theta_C, \phi_C)$ set to $(\pi/3 \text{ rad}; \pi/5 \text{ rad}; \pi/4 \text{ rad})$. Solving the position and orientation inverse kinematics problem in Section 2.2 results in four manipulator configurations, illustrated in Figure 5.

Figure 5 displays four inverse kinematic configurations for the end-effector position, each with unique workspaces and constrained joint angles. The bounds of these workspaces are determined by calculating the maximum distance from the origin coordinates to the end-effector using Figure 2. To save calculation time, the configuration workspace survey program omitted end-effector positions beyond the operating range, as defined by Equation (18).

$$\text{Max}_{\text{distance}} = \sqrt{d_1^2 + a_1^2} + AB + \sqrt{a_3^2 + (d_4 + d_6)^2} \quad (18)$$

In the next section, we will present the results of examining the workspaces of these inverse dynamic configurations, considering input parameters, space constraints, and mechanical joint angle limits, to assess their operational capabilities.

3.2 Workspace analysis

A manipulator's workspace is typically defined by its reachable positions across various inverse kinematic configurations, ignoring the directional angle. In Section 3.1, at point C, all four configurations are attainable with a fixed directional angle. However, not all calculated positions and orientations are feasible due to mechanical joint angle limitations. Additionally, joint angle constraints restrict the operational space of these configurations. This section clarifies this by conducting a two-step survey: first, we examine reachable working points for inverse configurations with a fixed direction angle to assess differences in their workspace. Second, we survey all working points while considering the direction angle, adjusting orientation to gauge configuration responsiveness. Throughout, we account for joint angle constraints to understand their impact on the inverse configuration's workspace.

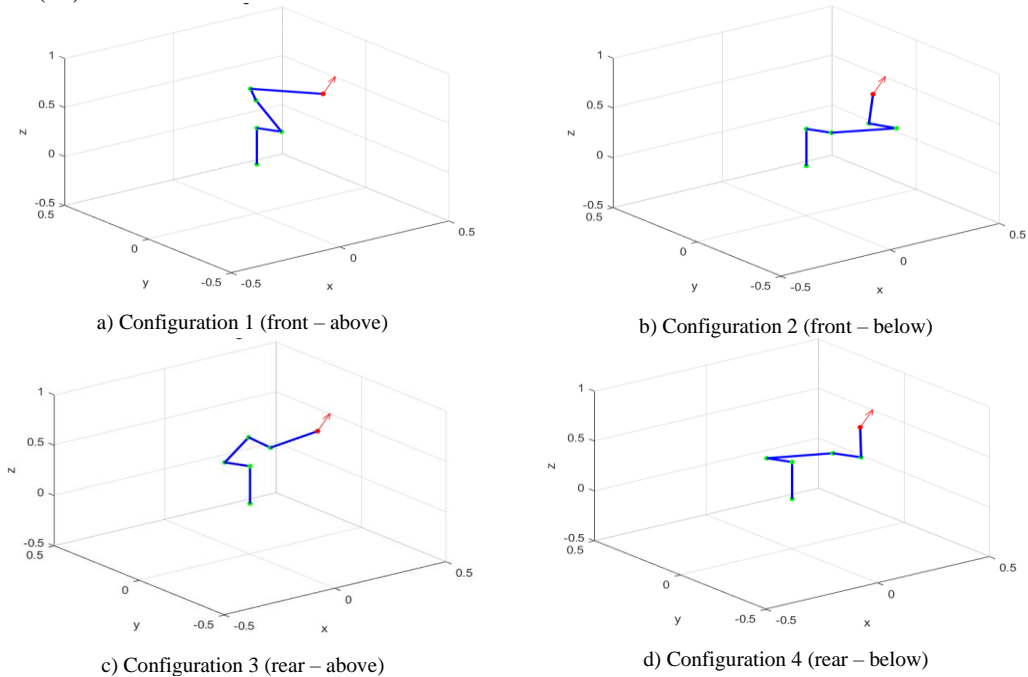
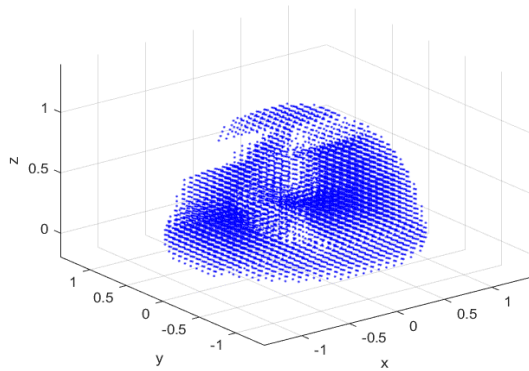
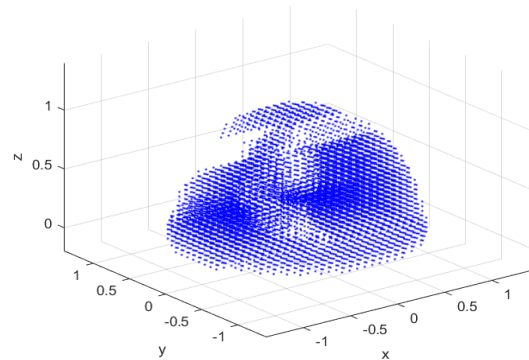


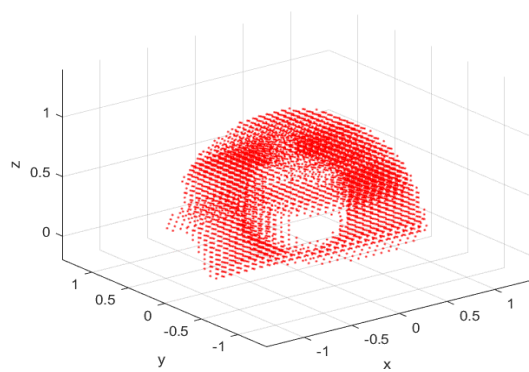
Figure 5 Four inverse configurations at point C (0.12 m; -0.24 m; 0.82 m) with respect to the orientation direction (red arrow) in the $Oxyz$ coordinates



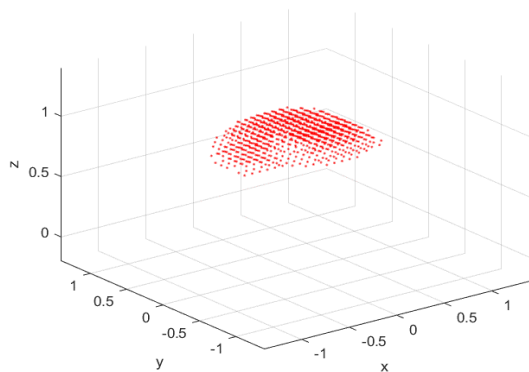
Workspace of configuration 1 with no joint limitation



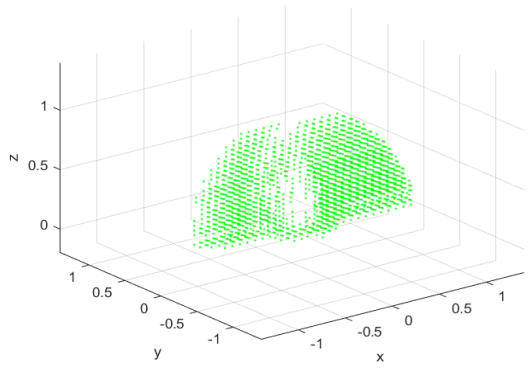
Workspace of configuration 1 with joint limitation



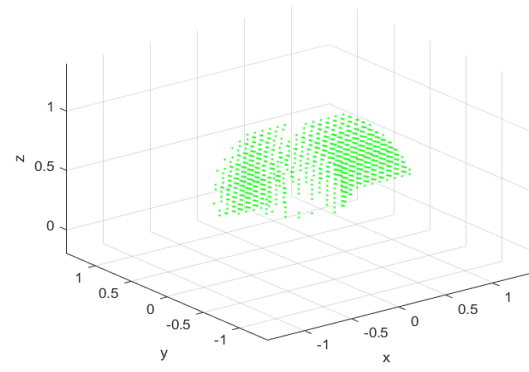
Workspace of configuration 2 with no joint limitation



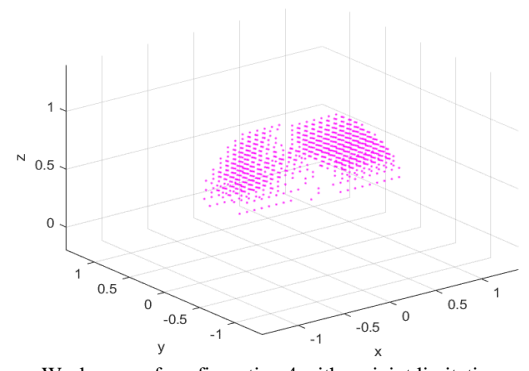
Workspace of configuration 2 with joint limitation



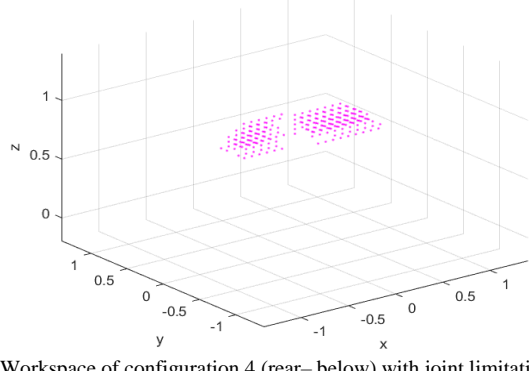
Workspace of configuration 3 with no joint limitation



Workspace of configuration 3 with joint limitation



Workspace of configuration 4 with no joint limitation



Workspace of configuration 4 (rear-below) with joint limitation

Figure 6 Workspace of four inverse configurations by position criteria with joint limitation

3.2.1 Position criteria

We conducted a workspace survey using the end-effector's position at a fixed orientation angle ($\psi=\pi/3$; $\theta=-\pi/3$; $\phi=\pi/4$) in two scenarios: one without considering joint angle limitations and another where we considered them for four inverse kinematic configurations (Isiah, & Luis, 2017). The surveyed space in Oxyz coordinates is bounded by the following limits:

$$-1.2(m) < x; y < 1.2(m); 0 < z < 1.2(m)$$

This space is divided into x , y , and z dimensions, forming a set of survey points for the end-effector. Each dimension is subdivided into 30 steps $x_{\text{step}}=y_{\text{step}}=z_{\text{step}}=30(\text{step})$. In the considered case, the joint angle limits are as follows:

$$-\pi \text{ (rad)} < \theta_1, \theta_4, \theta_6 < \pi \text{ (rad)}$$

$$-5\pi/6 \text{ (rad)} < \theta_2, \theta_3, \theta_5 < 5\pi/6 \text{ (rad)}$$

The survey results, presented in Figure 6 and Table 3, reveal variations in the number of working points (working space) for each inverse kinematic configuration. The workspaces of the configurations differ significantly in two cases: one where joint angle limitations are not considered (Figure 6a) and another where they are considered (Figure 6b).

Table 3 Workspace of four inverse configurations by position criteria

Configuration	No joint limitation (points)	Joint limitation (points)
1 (front – above)	6348	6146
2 (front – below)	4965	825
3 (rear – above)	1958	902
4 (rear – above)	805	225

Based on the survey results, the following observations stand out:

- Configuration 1 (front-above) has the most working points, while configuration 4 (rear-below) has the fewest working points in both scenarios.

- When considering joint angle limitations, the number of working points in the inverse configurations significantly decreases. For instance, in configuration 2 (front-below), the number of working points drops from 4965 points to 825 points, a reduction of over sixfold.

- The inverse kinematics configurations exhibit distinct workspace allocations within the surveyed area. These workspace distributions create interference zones and separate areas that are inaccessible to other configurations.

For a clearer illustration of the variations in working areas for each configuration, another survey was conducted using the position and orientation criteria of the proposed inverse kinematics problem. The results are presented and discussed in Section 3.3.

3.2.2 Position and orientation criteria

To survey the position and orientation inverse kinematics problem, we utilized the same input parameters as in Section 3.2. We defined the orientation angle for each surveyed end-effector position in XYZ dimensions based on roll, pitch, and yaw angles (ψ, θ, ϕ). Each angle (ψ, θ, ϕ), for rotation falls within the interval of $(-\pi/2, \pi/2)$ and is divided into 30 steps for a single survey calculation.

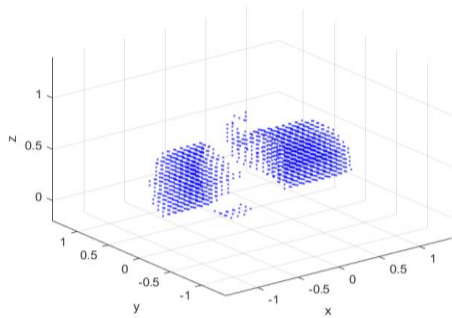
For each surveyed end-effector point, if the joint angles θ_i can satisfy all orientation angles examined at that position, it's recorded as a fully available working position in Oxyz coordinates. We conducted surveys for all four inverse configurations, both when disregarding and considering joint angle limitations, using the same scope and parameters for position and angles.

The survey results for the workspace, including fully available working points for all four inverse configurations, can be found in Table 4 and Figure 7.

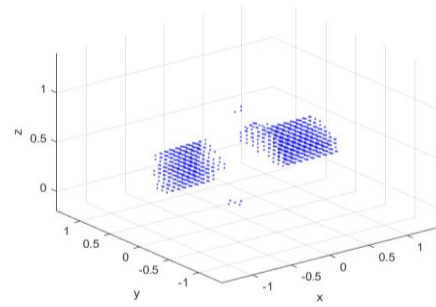
Table 4 Full-available workspace of four inverse configurations by position and orientation criteria

Configuration	No joint limitation (points)	Joint limitation (points)
1 (front – above)	1849	971
2 (front – below)	547	16
3 (rear – above)	91	26
4 (rear – above)	188	40

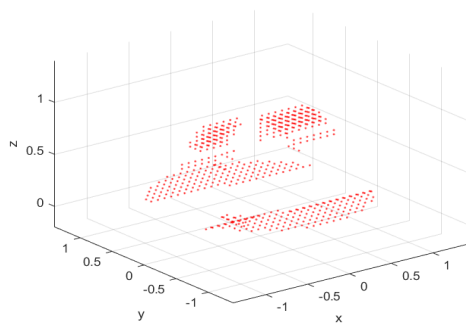
The results of the position and orientation inverse kinematics problem align with those in Section 3.2. Configuration 1 (front-above) achieved the highest number of full-available work points (1849), while configuration 3 (rear-above) had the lowest (91) when not considering θ_i limitations. When θ_i limitations are considered, the workspace for all configurations shrinks, particularly configuration 2, which reduces by over 34 times, from 547 points to 16 points. This underscores that, in practice, mechanical joint angle limitations are the primary factors limiting the 6-DOF manipulator's operational area.



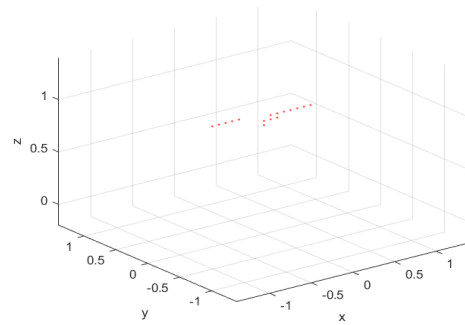
Full-available workspace of configuration 1 with no joint limitation



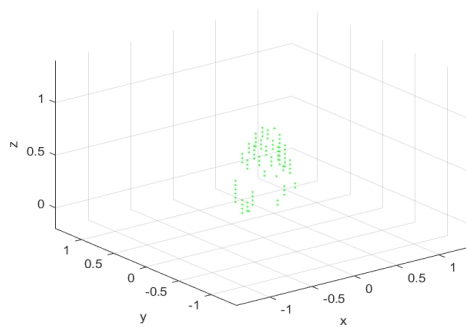
Full-available workspace of configuration 1 with joint limitation



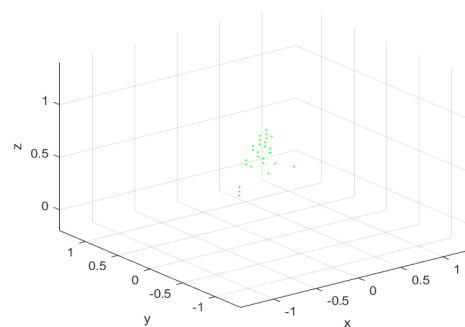
Full-available workspace of configuration 2 with no joint limitation



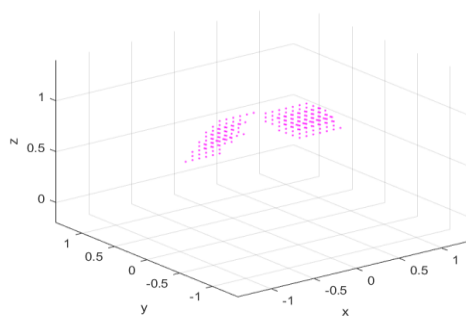
Full-available workspace of configuration 2 with joint limitation



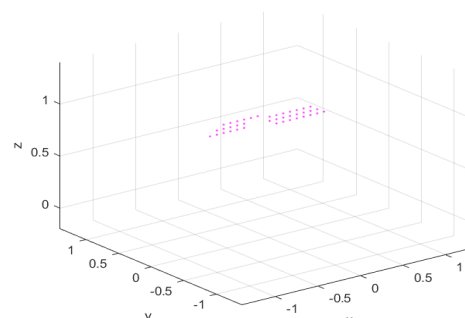
Full-available workspace of configuration 3 with no joint limitation



Full-available workspace of configuration 3 with joint limitation



Full-available workspace of configuration 4 with no joint limitation



Full-available workspace of configuration 4 with joint limitation

Figure 7 Full-available workspace of four inverse configurations by position and orientation criteria with joint limitation.

Considering the additional end-effector angle criteria in the second stage of the survey, the number of working points significantly decreased in both cases compared to the first stage. Furthermore, Figure 6 illustrates that the inverse kinematic configurations exhibit markedly different working regions than in the first stage.

Sections 3.2 and 3.3 reveal that the first configuration (front-above) offers the most extensive working space, even when joint angle limitations are taken into account. Typically, in training a 6-DOF manipulator for a specific task, this configuration is chosen based on expert experience. However, the survey results demonstrate that no single configuration can cover and access all working points and angles in space when considering both the manipulator's position and orientation.

Consequently, in intelligent robot applications where the environment is dynamic, robots must not only adhere to predefined procedures but also possess the ability to select an inverse configuration from their distinct workspaces. In the following section, we explore proposals for a novel approach to selecting inverse kinematic configurations for 6-DOF manipulators in end-effector path planning.

4. Automated inverse kinematics configuration selection

As mentioned in Section 3, inverse kinematics configuration 1 has the largest working area and is commonly used as the primary configuration for controlling repetitive operations, especially in production lines. However, the

working areas of the inverse kinematic configurations are distinct, and no single configuration can encompass all end-effector positions and orientations. In certain scenarios, it's necessary to move the manipulator's end-effector along a path or with an orientation that lies outside the primary configuration's active area. Several publications have addressed trajectory planning for 6-DOF manipulators (Perumaal, & Jawahar, 2012; Siméon et al., 2004; Gracia et al., 2009).

This section outlines an algorithm for choosing inverse kinematic configurations in the path planning of a 6-DOF robot. To assess the suitability of each inverse kinematic configuration, we propose a trajectory for the manipulator's position and orientation. The survey findings, along with the algorithm for selecting the appropriate configuration (among multiple solutions), based on the minimum number of state transitions criterion, are presented.

The end-effector's trajectory, comprising position (x, y, z) and orientation (ϕ, θ, ψ) , is described by Equations (19, 20) and depicted in Figure 8, with the parameter t divided into n equally spaced points (20 and 1000 points) to create survey segments along the end-effector's path.

$$\begin{aligned} x(t) &= 0.4\sin(t)\sin(5t); \\ y(t) &= 0.4\sin(t)\cos(4t); \\ z(t) &= 0.4\cos(t)+0.5 \end{aligned} \quad (19)$$

$$\begin{aligned} \phi(t) &= 0.1\sin(t)\cos(0.1t); \\ \theta(t) &= 0.1\sin(t)\cos(0.1t); \\ \psi(t) &= 0.1\sin(t)\cos(0.2t) \end{aligned} \quad (20)$$

where $0 < t < 2\pi$

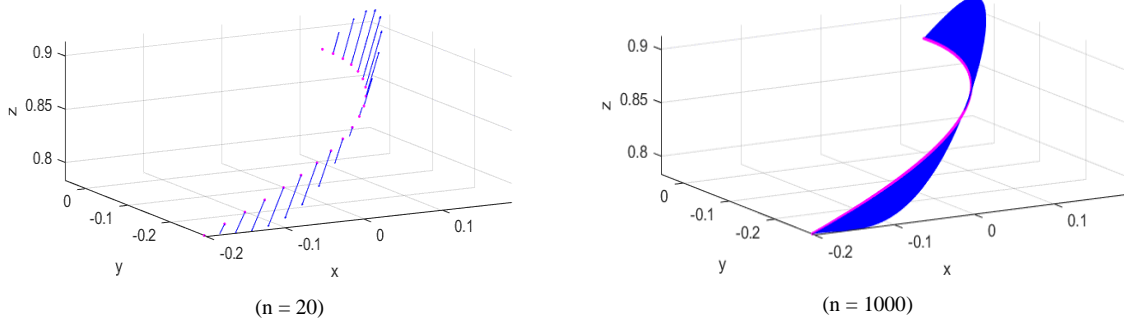


Figure 8 End-effector positions (red dots) and orientations (blue arrows) along the path for both $n = 20$ and $n = 1000$ cases

Conduct a survey on the suitability of inverse kinematic configurations based on the locus of the point and the orientation using equations 19-20 with the number of points divided by 1000. Figure 9 illustrates the working area of four inverse kinematics configurations and the path. Table 5 shows the results of the available inverse kinematic configurations with the point segments.

Table 5 The compatibility of four inverse configurations on a point locus segment

Configuration	Available point segment (from point to point)
1	532-1000
2	1-457
3	389-873
4	168-436

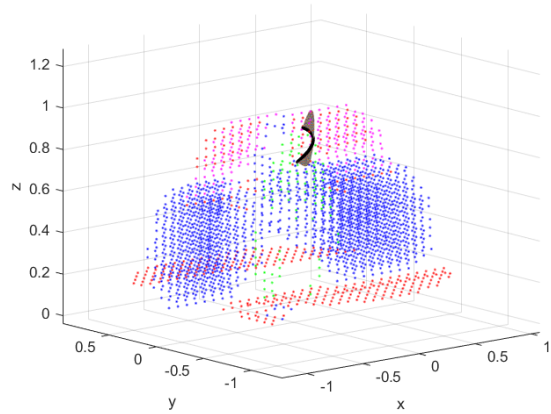


Figure 9 Full-available workspace for all four inverse configurations and the path of the end-effector's position and orientation

Note: Configuration 1: blue dot; configuration 2: red dot; configuration 3: green dot; configuration 4: magenta dot; locus path: black line with brown vector.

Figure 9 and Table 5 demonstrate that individual configurations do not cover the entire end-effector trajectory. Configuration 1, as shown in Table 5, only applies from the 532nd to the 1000th point. Consequently, a fixed inverse kinematic configuration based on the largest workspace criterion is not feasible. Additionally, neither configuration group 1-2 nor 3-4 spans the entire trajectory, necessitating the robot to switch between front and rear configurations to traverse the full path. Completing the trajectory provides numerous options with compatible inverse configurations at the same point. Without an appropriate selection mechanism, this could lead to

numerous configuration transitions, which is detrimental to the control process.

This paper presents an algorithm to automatically select the most suitable inverse kinematic configurations for path planning, aiming to minimize configuration transitions. The algorithm consists of the following steps:

Step 1: Survey the locus using four inverse kinematic configurations and calculate the available segments for each.

Step 2: Select the priority configuration pair (front or rear configurations) with the longest segments along the specified locus.

Step 3: Create the path plan using the priority pair configuration, with switching points at the beginning and end of the determined segment of the preferred configurations. If necessary, empty path segments will be filled with the matching configuration from the remaining pair of configurations.

Step 4: Adjust the path plan to reduce the number of configuration transitions based on the criteria function.

Figure 10 illustrates the results of applying the algorithm to the data presented in Table 5 for the purpose of selecting inverse kinematic configurations. Among the available options, the front configuration pair (comprising configurations 1 and 2) stands out, offering the longest path. This path encompasses 925 configurations, stretching from the 1st point of configuration 2 to the 457th point and from the 523rd point of configuration 1 to the 1000th point. In contrast, the rear configuration pair (consisting of configurations 3 and 4) covers 705 configurations, spanning from the 168th to the 436th point of configuration 4 and from the 389th point to the 873rd point of configuration 3. These distinct point segments are depicted using dashed lines.

As a result, priority is given to the front configuration pair for path planning. This front pair is emphasized with a continuous blue line, indicating transition points at the initial point, the 457th point, the 532nd point, and the endpoint at the 1000th point.

Figure 11 depicts the inverse kinematic configurations at these transition points. The locus initiates with configuration 2 at the first point (Figure 11.a), transitions to configuration 3 at the 457th point (Figure 11.b), and maintains this configuration until shifting to configuration 1 at the 532nd point (Figure 11.c). The robot operates in

configuration 1 and concludes at the 1000th point (Figure 11.d). The proposed algorithm results in two configuration transitions at the 457th point and 532nd point.

Algorithm Path planning with multi-configuration selection	
Require: workspace of four inverse configurations, end-effector locus	
Ensure: Minimizing the number of configuration transitions	
1:	procedure Path planning
2:	for i =1 to 4 (configuration) do
3:	for j: =1 to 1000 (n points) do
4:	if point and orientation is available then
5:	record (i, j)
6:	end
7:	end
8:	segments(i) = available (record (i,:))
9:	end
10:	priority_pair = max (segment (1-2;3-4))
11:	sw_points_temp = edge of priority segments
12:	path_planning_temp = start point → sw_points_temp → end point
13:	criteria = number of configuration transitions
14:	while criteria is not minimum do
15:	update sw_points_temp
16:	path_planning = start point → sw_points_temp → end point
17:	criteria = number of configuration transitions
18:	end

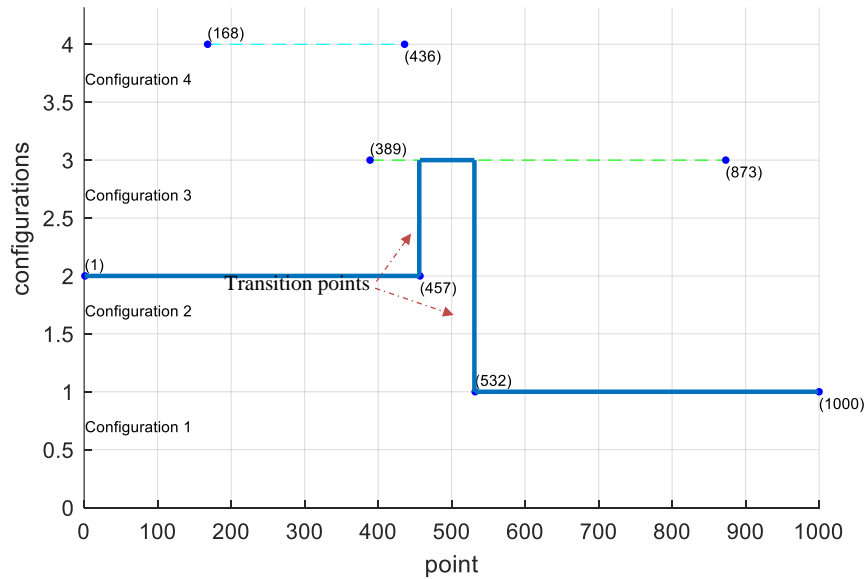


Figure 10 Selection of the inverse configurations for path planning

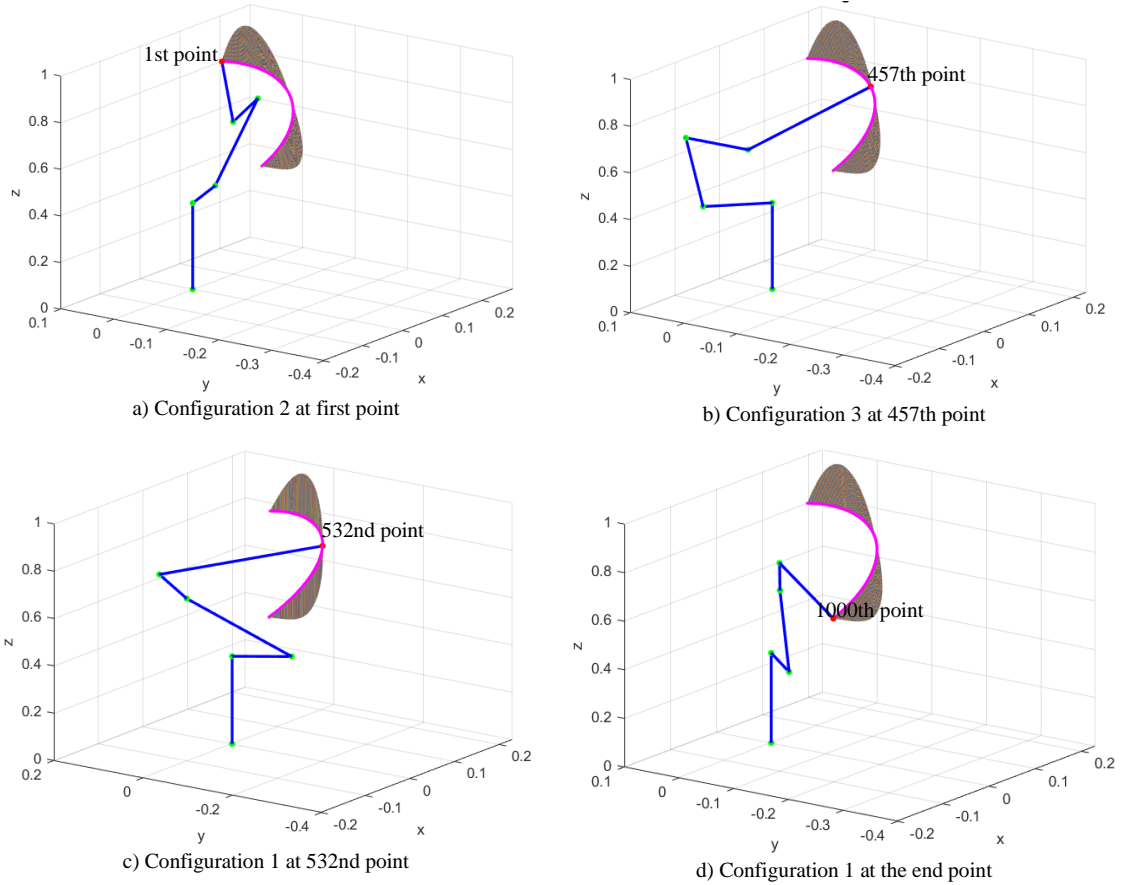


Figure 11 Selected inverse configuration at transition points.

To test the practicality and effectiveness of the proposed algorithm for automatic configuration selection, it was applied to different paths of end-effector position and orientation (from Experimental 2 to Experimental 4). Figure 12 displays the survey results, including the position and orientation functions, as well as the automatic configuration selection.

The survey results in Figures 11 and 12, covering various end-effector position and orientation functions, lead to the following conclusions:

- Various segments match inverse kinematic configurations according to the end-effector's position and orientation along the path.

- Configuration selection is necessary at specific switching points due to potential overlaps and varying segment lengths.

- Select suitable segments carefully to maintain continuous motion from the path's start to end, prioritizing configuration pairs with the most compatible segments.

- The auto-configure algorithm efficiently pinpoints switching points, minimizes transitions, and ensures stable, smooth control of the 6-DOF robot manipulator.

This algorithm's architecture seamlessly integrates into autonomous robot controllers, enabling adaptability to new environments and potentially replacing expert-based pre-programmed controls. This adaptability extends to medical, defense, and rescue operations.

Experimental 2).

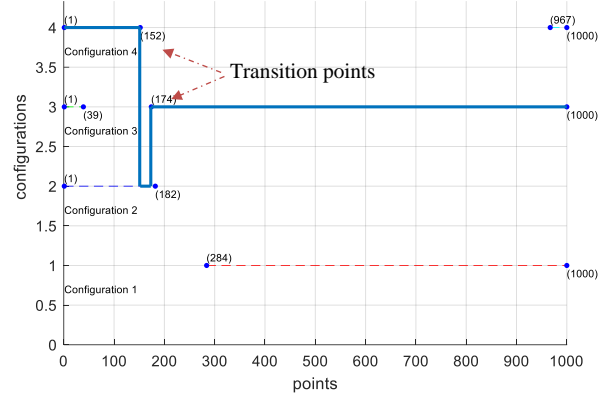
Position functions: where $\pi/10 < t < \pi/4$

$$\begin{aligned} x(t) &= 0.4\sin(t)\sin(6t); \\ y(t) &= 0.4\sin(t)\cos(6t); \\ z(t) &= 0.4\cos(t)+0.4 \end{aligned}$$

Orientation functions: where $0 < t < 2\pi$

$$\begin{aligned} \phi(t) &= 0.2\sin(t)\cos(0.2t); \\ \theta(t) &= 0.2\sin(t)\cos(0.2t); \\ \psi(t) &= 0.4\sin(t)\cos(0.2t) \end{aligned}$$

Note: The path (blue line) starts with configuration 4 at the initial point, transitions to configuration 2 at point 152, shifts to configuration 3 at point 174, and concludes at point 1000. This results in two configuration transitions at points 152 and 174.



a) Experimental 2: The rear configuration pair (configuration 3 and 4) is preferred.

Experimental 3:

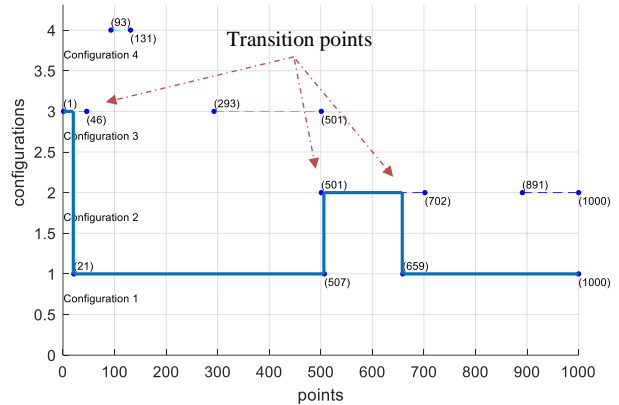
Position functions: where $-\pi/2 < t < \pi/2$

$$\begin{aligned} x(t) &= 0.4\sin(t); \\ y(t) &= 0.5x(t); \\ z(t) &= 0.4\cos(t)+0.48; \end{aligned}$$

Orientation functions: where $0 < t < 2\pi$

$$\begin{aligned} \phi(t) &= 0.1\sin(t)\cos(0.1t); \\ \theta(t) &= -0.1\sin(t)\cos(0.1t); \\ \psi(t) &= -0.2\sin(t)\cos(0.2t); \end{aligned}$$

Note: The path (blue line) starts with configuration 3 at the initial point, switches to configuration 1 at point 21, shifts to configuration 2 at point 507, returns to configuration 1 at point 659, and concludes at point 1000. This results in three configuration transitions at points 21, 507, and 659.



b) Experimental 3: The front configuration pair (configuration 1 and 2) is preferred.

Experimental 4:

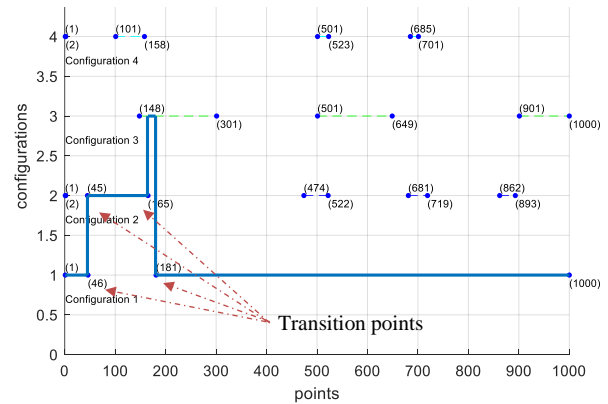
Position functions: where $0 < t < \pi/2$

$$\begin{aligned} x(t) &= 0.4\sin(t)\sin(10t); \\ y(t) &= 0.4\sin(t)\cos(10t); \\ z(t) &= 0.4\cos(t)+0.5; \end{aligned}$$

Orientation functions: where $0 < t < 2\pi$

$$\begin{aligned} \phi(t) &= 0.1\sin(t)\cos(0.1t); \\ \theta(t) &= -0.1\sin(t)\cos(0.1t); \\ \psi(t) &= -0.2\sin(t)\cos(0.2t); \end{aligned}$$

Note: The path (blue line) starts with configuration 1 at the beginning, transitions to configuration 2 at the 46th point, shifts to configuration 3 at the 165th point, reverts to configuration 1 at the 181st point, and ends at point 1000. This results in three configuration transitions occurring at points 46, 165, and 181.



c) Experimental 4: The front configuration pair (configuration 1 and 2) is preferred.

Figure 12 Automated inverse kinematic configuration selection for various path planning

5. Conclusion

In this paper, we delve into the kinematics of a six-degree-of-freedom robot configuration. We conquered the challenge of forward kinematics by employing the Denavit-Hartenberg matrix method. Additionally, we simplified the intricate problem of multi-solution inverse kinematics through geometric analysis, breaking it down into two critical stages: calculation and angle solution selection.

To facilitate our simulation survey, we designed a dedicated computer program for simulating the robot's operational configurations. Our survey revealed a variety of working points in space for inverse configurations, accounting for joint angle constraints. Importantly, we highlighted the reduction in the robot's operational workspace when considering joint angles.

To address diverse path planning scenarios, we introduced an algorithm capable of autonomously selecting the most suitable inverse kinematic configurations. Our results showcased the robot's adeptness at automatic and efficient configuration switching, aimed at minimizing transitions. This algorithm shows promise for application in intelligent robotic systems and unfamiliar environments. Our upcoming research will delve into the topic of using intelligent algorithms to plan paths for 6-degree-of-freedom robots.

6. References

- Abderrahim, B., Moulay, E. H. E. C., Hassan S., & Hicham A. E., (2023). The Inverse Kinematics Evaluation of 6-DOF Robots in Cooperative Tasks Using Virtual Modeling Design and Artificial Intelligence Tools. *The International Journal of Robotics Research*, 12(2), 121-130. <https://doi.org/10.18178/ijmerr.12.2.121-130>
- Ahmed, R. J. A., Canan, D. L., & Sadettin, K. (2016). A New Artificial Neural Network Approach in Solving Inverse Kinematics of Robotic Arm (Denso VP6242). *Computational Intelligence and Neuroscience*, 2016, Article 5720163. <https://doi.org/10.1155/2016/5720163>
- AKB Machinery. (n.d.). *AKB-IRV1 6-DOF robot*. Retrieved from <https://akbmachinery.com/san-pham/canh-tay-robot-6-bac-tu-do-akb-irv1/>
- Chemuly, V. V. M. J. S., & Voruganti, H. K. (2020). An efficient approach for inverse kinematics and redundancy resolution of spatial redundant robots for cluttered environment. *SN Applied Sciences*, 2, Article 1012. <https://doi.org/10.1007/s42452-020-2825-x>
- Chen, Q., Zhu, S., & Zhang, X. (2015). Improved Inverse Kinematics Algorithm Using Screw Theory for a Six-DOF Robot Manipulator, *International Journal of Advanced Robotic Systems*, 12(10), Article 60834. <https://doi.org/10.5772/60834>
- Craig, J. J. (2005). *Introduction to Robotics: Mechanics and Control* (3rd ed.). New Jersey: Prentice Hall.
- Denavit, J. & Hartenberg, R. (1955). A Kinematic Notation for Lower-Pair Mechanisms Based on Matrices. *Journal of Applied Mechanics*, 22(2), 215–221. <https://doi.org/10.1115/1.4011045>
- Gasparetto, A., Boscariol, P., Lanzutti, A., & Vidoni, R. (2015). Path Planning and Trajectory Planning Algorithms: A General Overview. In: Carbone, G., Gomez-Bravo, F. (eds) *Motion and Operation Planning of Robotic Systems. Mechanisms and Machine Science*, 29. Cham: Springer, https://doi.org/10.1007/978-3-319-14705-5_1
- Gracia, L., Andres, J. & Tornero, J. (2009). Trajectory Tracking with a 6R Serial Industrial Robot with Ordinary and Non-ordinary Singularities. *International Journal of Control, Automation, and Systems*, 7, 85-96. <https://doi.org/10.1007/s12555-009-0111-1>
- Hartenberg, R. & Denavit, J. (1964). *Kinematic Synthesis of Linkages* (1st ed.). McGraw Hill.
- Hayes, M. J. D., Husty, M. L., & Zsombor-Murray, P. J. (2003). Singular Configurations of Wrist-Partitioned 6R Serial Robots: A Geometric Perspective for Users. *Transactions of the Canadian Society for Mechanical Engineering*, 26(1), 41-55. <https://doi.org/10.1139/tcsme-2002-0003>.
- Husi, G. (2015). Position Singularities and Ambiguities of the KUKA KR5 Robot. *International Journal of Engineering*

- Technologies IJET*, 1(1), 44–50.
<https://doi.org/10.19072/ijet.105700>
- Iqbal, J., Islam, R. & Khan, H. (2012). Modeling and Analysis of a 6 DOF Robotic Arm Manipulator. *Canadian Journal on Electrical and Electronics Engineering*, 3(6), 300–306.
- Isiah, Z. & Luis, B. (2017). A novel closed-form solution for the inverse kinematics of redundant manipulators through workspace analysis. *Mechanism and Machine Theory*, 121, 829–843.
<https://doi.org/10.1016/j.mechmachtheory.2017.12.005>
- Kshitish, K. D., Bibhuti, B. C., & Sukanta, K. S. (2017). A Inverse Kinematic Solution Of A 6-DOF Industrial Robot Using ANN. *Indian Journal of Social Science Research*, 15(2), 97–101
- Lee, C. S. G., & Ziegler, M. (1984). A Geometric Approach in Solving the Inverse Kinematics of Puma Robots. *IEEE Transactions on Aerospace and Electronic Systems*, AES-20(6), 695–706.
<https://doi.org/10.1109/TAES.1984.310452>
- Perumaal, S. S., & Jawahar N. (2012). Automated Trajectory Planner of Industrial Robot for Pick-and-Place Task. *International Journal of Advanced Robotic Systems*, 10(2), Article 53940. <https://doi.org/10.5772/53940>
- Piotrowski, N., & Barylski, A. (2014). Modelling a 6-DOF Manipulator using Matlab software. *Archives of Mechanical Technology and Automation*, 34(3), 45–55
- Siméon, T., Laumond J. P., Cortés, J., & Sahbani A. (2004). Manipulation Planning with Probabilistic Roadmaps. *The International Journal of Robotics Research*, 23(7–8), 729–746.
<https://doi.org/10.1177/0278364904045471>
- Spong, M. W., Hutchinson, S., & Vidyasagar, M., (2020). *Robot Modelling and Control* (2nd ed.), New Jersey: John Wiley & Sons, Inc.
- Spong, M. W., Hutchinson, S., & Vidyasagar, M., (2004). *Robot Dynamic and Control*. (2nd ed.), Academia.edu Publishing.
- Tagliani, F. L., Pellegrini, N., & Aggogeri, F. (2022). Machine Learning Sequential Methodology for Robot Inverse Kinematic Modelling. *Applied Sciences*, 12(19), 9417. <https://doi.org/10.3390/app12199417>.
- Wang, X., Zhang, D., & Zhao C., (2017). The inverse kinematics of a 7R 6-degree-of-freedom robot with non-spherical wrist. *Advances in Mechanical Engineering*, 9(8). <https://doi.org/10.1177/1687814017714985>
- Wang, X., Cao, J., Chen, L., & Hu, H. (2020). Two Optimized General Methods for Inverse Kinematics of 6R, Robots Based on Machine Learning. *Mathematical Problems in Engineering*, 2020, Article 8174924. <https://doi.org/10.1155/2020/8174924>.
- Yiyang, L., Xi, J., Hongfei, B., Zhining, W. & Liangliang, S. (2021), A General Robot Inverse Kinematics Solution Method Based on Improved PSO Algorithm. *IEEE Access*, 9, 32341–32350. <https://doi.org/10.1109/ACCESS.2021.3059714>
- Zhang, D. & Hannaford, B. (2019). IKBT: solving symbolic inverse kinematics with behavior tree. *Journal of Artificial Intelligence Research*, 65(1), 457–486. <https://doi.org/10.1613/jair.1.115>